Silicon Controlled Drift Detectors for Imaging Applications

A. Castoldi
Politecnico di Milano, Dipartimento di Ingegneria Nucleare Ce.S.N.E.F., 20133 Milano, Italy and INFN, Sezione di Milano, Italy

C. Guazzoni
Politecnico di Milano, Dipartimento di Elettronica e Informazione, 20133 Milano, Italy and INFN, Sezione di Milano, Italy

S. Masci
Politecnico di Milano, Dipartimento di Elettronica e Informazione, 20133 Milano, Italy

R. Hartmann
PN Sensor GmbH, Roemer Strasse 28, München D-80803, Germany

L. Strüder
Max Planck Institut für Extraterrestriche Physik, Otto-Hahn-Ring 6, München D-81739, Germany

The Controlled Drift Detector (CDD) is the more recent evolution of silicon drift detectors for 2D position sensing and spectroscopy of X-rays. Among the novel features, the signal charge is forced to drift within arrays of separate drifting channels, the activation of the drift field can be controlled externally, and the precise timing of the interaction is obtained from the fast signal induced on the back electrodes by the initial motion of the electron-hole pairs. These features allow 2D position information with high resolution and reduced number of channels, readout time of a full detector frame of a few microseconds and measurement of the deposited energy with spectroscopic resolution. The potential of such detectors has been confirmed by the experimental characterization and the achievable performance in x-ray imaging and spectroscopy tests will be presented. 2D images of the ionization profile of charged particles will also be shown together with the first results of the characterization of a new large area CDD prototype.

1. INTRODUCTION

Since the invention of Silicon Drift Detectors [1] in 1983 by Gatti and Rehak as two dimensional position-sensitive detectors for ionizing particles we have assisted to a substantial evolution in detector technology, architecture and performance. As a consequence Silicon Drift Detectors have been employed as particle tracking detectors in high-energy physics experiments [2-4] and opened to novel field of application in high-resolution X-ray spectroscopy and imaging [5, 6].

The needs of X-ray spectroscopy drove the design towards circular topologies with central anode and on-chip JFET [6] as well as towards monolithic arrays of SDD cells in order to achieve larger active areas and higher count rates [7]. Such arrays can also provide low resolution imaging with position resolution limited by the size of each cell (at best of the order of 1 mm). Recently asymmetric topologies (with droplet-like shape) with the anode and the JFET shifted to the side of the structure improved the achievable peak-to-background ratio (typically of the order of 1500 with standard 5 mm^2 SDDs with symmetric round shape and concentric drift rings and of 3000 with 10 mm^2 SDDs) [8]. The asymmetric anode layout has a two-fold advantage as it allows shielding the readout section from the incident radiation and allows the optimization of the anode-JFET noise performance. Excellent results have been obtained with this detector both in terms of energy resolution (128 eV FWHM at the Mn Kα line at -15 °C with a 5 mm^2 detector) and of peak-to-background ratio (about 7000 for 5 mm^2 detector and 10000 for 10 mm^2 detector). However, the required shielding structure makes it difficult to develop large monolithic matrixes with minimized dead area using the Silicon Drift Detector droplet as the basic cell.

We have designed in the last decade novel architectures of multi-anode silicon drift detectors with linear geometry (Multi-Linear Silicon Drift Detectors - ML-SDDs) [9] and of Controlled-Drift Detectors with the aim to extend the potential of Silicon Drift Detectors to X-ray imaging with high energy- and time-resolution. The linear structure naturally accounts for the noise optimization of the anode capacitance and JFET structure but it also allows the development of large area multi-channel detectors where the readout sections are outside the active area and can be easily shielded to avoid the spoiling of the peak-to-background ratio.

These novel detector topologies are good candidates to fulfill the new frontier in sensitivity, energy range and time resolution posed by the recent development in synchrotron light sources. Recently we have used these detectors to track Compton electrons within a single detector layer.

In this paper we describe the innovative features of Silicon Controlled Drift Detectors with respect to conventional silicon drift detectors (Section 2). Section 3 reviews the performance achievable with this detector family and Section 4 shows examples of application of these detectors in advanced imaging techniques.

2. THE SILICON CONTROLLED DRIFT DETECTOR CONCEPT

2.1. Detector working principle

The Controlled Drift Detector (CDD) was proposed in 1997 [10, 11] as a novel detector topology which features

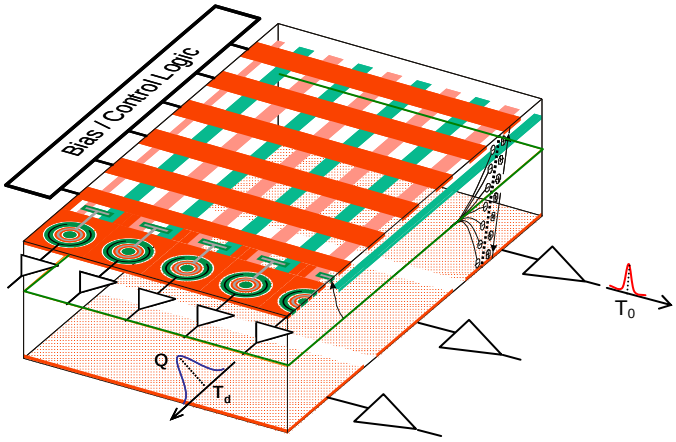

Figure 1. Sketch of the Controlled-Drift Detector structure. Five drifting columns are shown with their readout section (collecting anode and integrated JFET). The amplitude (Q) and arrival time (T_d) of the shown pulse give the deposited energy and incident position.

2-D position resolution and energy spectroscopy of X-rays in the range 1-30 keV with full frame duration of few tens of μs. The detector, whose structure is schematically shown in Figure 1, is built on a fully depleted high-resistivity silicon wafer (typically 300-450 μm thick) that assures good quantum efficiency in the 1-30 keV range. The detector working principle is based on the generation of equally spaced potential wells along the drift direction during the integration phase and on the transport of the charge packets stored in each pixel by means of an electrostatic field during the readout phase (integrate-readout mode). The required potential distribution within the first micrometers below the detector surface is obtained by a suitable combination of electrode layout, bias voltages and buried doped regions.

The removable potential barrier controlling the drift of the electron charge is provided by an externally controlled perturbation applied to the linear drift potential. The permanent confinement in the direction transversal to the drift is obtained with a suitably tailored pattern of deep p and n implants. The detector operates in single-photon counting mode that is, for each detected X-ray photon, the incident position along the drift direction is given by the measurement of the electron drift time while the X-ray energy is obtained from the measurement of the collected charge. The second spatial coordinate is obtained from the granularity of the readout anodes. The size of the anodes, and therefore their capacitance, can be made very small (of the order of 100 fF) and independent of the whole active area of the detector as in a conventional Silicon Drift Detector [6]. This, in conjunction with the availability of on-chip front-end electronics, allows a low noise measurement of the time of arrival as well as of the amplitude of the signal charge. Drift velocities in the range 0.3-0.5 cm/μs have been measured and lead to readout times of the order of 2-3 μs for a 1 cm-long detector. This readout mechanism allows integration times of only few tens of μs that is inherently faster than a Charge-Coupled Device [12] which represents the reference device for high-resolution imaging and spectroscopy of X-rays. This feature allows operating the CDD at room temperature while having an energy resolution close to the one obtainable with state-of-the-art Charge-Coupled Devices typically operating at cryogenic temperatures and lower frame frequency [12]. For more demanding spectroscopic applications an energy resolution close to the ultimate value can be reached by moderately (Peltier) cooling the detector (e.g. close to 0°C).

If the energy resolution is the main concern, the detector can be operated in continuous readout mode (i.e. as a Self-Triggered Multi-Linear Silicon Drift Detector [13]). In this operating condition the detector features parallel columns permanently biased in drift mode thus retaining a 1-D position resolution. This results in a dramatic improvement in the achievable energy resolution at room temperature – since there is no integration of the leakage current– and in the possibility to operate at very high rates. With respect to Silicon Drift Detector arrays [7] – formed by a matrix of hexagonal (or rectangular) SDD macro-cells – this topology is particularly suitable to optimize the signal-to-noise ratio of the readout section because the anode size can be reduced in order to minimize dead area and to improve the achievable peak-to-background ratio. Moreover in the first ns after generation the electron-hole pairs induce a fast signal on the back electrodes that can be used as a start trigger for the electron drift to achieve 2-D position sensing even in continuous readout mode although the low energy threshold increases to a few keV [13,14]. The choice between the two operating modes however does not even require switching off the detector thus offering a high degree of flexibility in the experimental phase.

The photon flux incident on the detector is limited by the occurrence of pulse pile-up. When the analog shaping time is much greater than the drift time only one event per column is allowed to avoid pile-up. On the other side when the shaping time is much smaller than the drift time more events can be stored in one column, the maximum occupancy being eventually limited by charge broadening (for X-rays typically less than 150 μm rms for a 1cm detector length). In this case a more sophisticated multiple-pulse processor is needed [15]. The acquisition system used for the measurements presented in this paper requires that only one photon hits the detector column per frame.

2.2. Designed structures

We have designed several prototypes of Controlled Drift Detectors/Silicon Drift Detectors featuring different active areas and different pixel sizes. All the designed prototypes have been produced at the Halbleiterlabor of the Max Planck Institut in cooperation with PNSensor GmbH. Two different pixel topologies have been implemented. In the first pixel prototype, having six strips per pixel, the biasing scheme for the integration mode is obtained by means of three resistive dividers, each one being connected to two

strips of the pixel. In the second one the pixel length is 120 µm corresponding to a cell of 4 strips. The corresponding voltage pattern during integration is obtained with only two dividers, thus simplifying both design and interconnections. There is margin to tailor the pixel size according to experimental needs down to a size of about 60 µm.

The largest device we have designed and that is presently under test is a 3×1 cm^2 detector with a pixel size of 120 µm. It features 240 anodes with on-chip front-end JFET and a maximum drift length of about 1 cm. The p^+ junction on the backside has been segmented in 15 strips.

For all of the prototypes the detector design is such that it can be operated either in continuous readout mode, using the induction signal from the back as the start-time to measure the drift time, or in integrate-readout mode (i.e. as a Controlled Drift Detector) thanks to the availability of different voltage dividers able to bias the field strips according to the bias scheme chosen to create the surface perturbation.

3. PERFORMANCE EVALUATION

We have qualified the performance achievable with this kind of detector in terms of energy resolution, position resolution and timing capability [16-19] with extended tests in the lab and with synchrotron light on different CDD prototypes with active areas up to 6x6 mm^2. A dedicated data acquisition system has been developed [20] to cope with the particular requirements of this kind of detector and suitable for data acquisition both in integrate-readout and in continuous readout modes. In the first sub-section we summarize the achievable performance and in the second one we present the functionality tests carried out on the large area prototype.

3.1. Energy, position and timing resolution

Figure 2 shows position-sensing and spectroscopic capability of a 4mm x 6mm CDD prototype (pixel size 180µm × 180µm). The detector was operated at 67 kHz

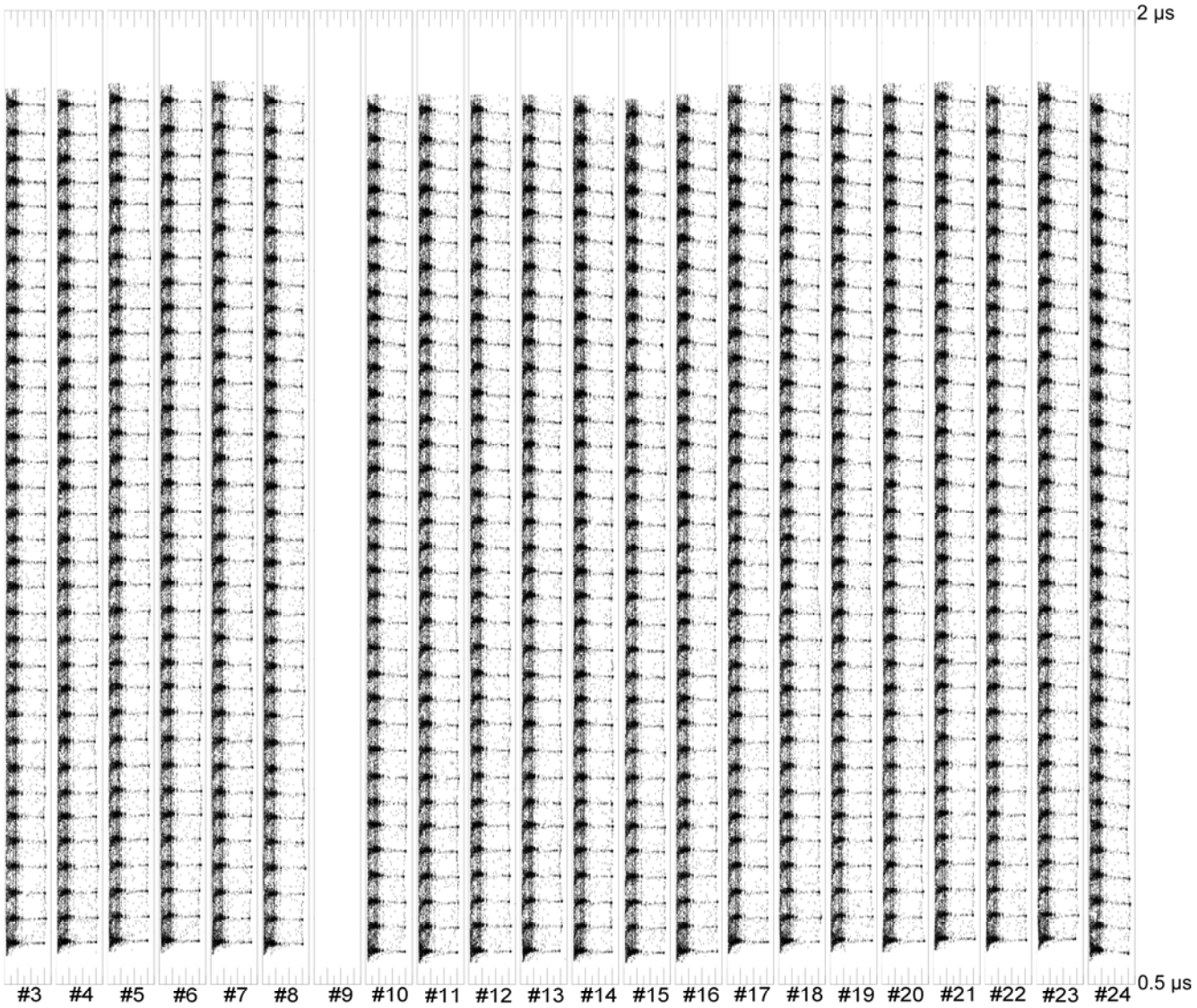

Figure 2. Flat image of a ^{241}Am source collected by a 180µm-pixel CDD prototype at room temperature. The frame frequency is 67 kHz. For each drift channels, the scatter plot energy-drift time is reported in the energy window 10-60 keV.

frame frequency and was irradiated with a ^{241}Am source. Channel #9 is missing due to an accidental damage occurred during tests. The individual pixels are well separated along the time axis over the whole active area demonstrating that the integrate-readout mode allows precise measurement of the electron drift time and therefore of the interaction coordinate. The energy resolution achieved with this prototype at room temperature is limited to 1.2 keV FWHM at the 13.9 keV Np line, due to an excess of leakage current. By moderately cooling down the detector (T=240K) the energy resolution improves to 300 eV FWHM and the drift time from the farthest pixel reduces to 0.8μs, thus allowing the operation of the detector at 125kHz frame rate.

The timing capability of the CDD has been successfully tested by imaging the X-rays shaped by a mask vibrating at acoustic frequency with a time resolution down to 10μs [21]. Such capability of time-resolved full-frame imaging is limited to periodic phenomena.

The achievable time resolution of the trigger signal is limited by the electronic noise (i.e. by the total readout capacitance) and by the random properties (i.e. energy, interaction position) of the recoil electron. In [14] we reported a measured time resolution of 1.5 ns rms for laser-generated (904 nm wavelength) signal charge of about 30,000 electrons in the case of total capacitance of the readout node ($C_{strip}+C_{stray}$) of the back side about 10 pF (measured). In the same paper we estimated that the contribution of random ionization depth is about 3 ns in a 300 μm thick wafer. With an induced charge on the back electrode of about 3,000 electrons (12.5keV), a time jitter below 10 ns can be obtained.

3.2. Functionality tests on the 3cm^2 CDD

We have tested the operation of the 240 on-chip JFETs by measuring the DC (saturation current and pinch-off voltage) and the small signal parameters (transconductance and output resistance). Figure 3 shows the histograms relative to the trasconductance and the output resistance. The spread of the parameters is below 3%.

Preliminary tests of the electron transport over the full 1 cm drift length have been carried out. An infrared pulsed laser (904 nm) has been focused on the front side of the CDD in the middle of one drift channel to generate the signal charge. A shaping time of 250 ns was used for the measurement. We displaced the laser by 120 μm steps (equal to 4 times the pitch of the field strips) along the drift direction. Figure 4 shows the drift time as a function of the drift coordinate with the CDD biased at 450 V/cm. Proper electron drift is achieved over the full detector length at an average velocity of about 83% of the nominal drift velocity (i.e. mobility times the average drift field). Less than 2 μs are required to readout the signal charge coming from the farthest edge of the detector and even shorter readout times can be obtained by increasing the drift field. We also tested the detector in integrate-readout mode and proper operation has been obtained both in charge confinement and in charge readout.

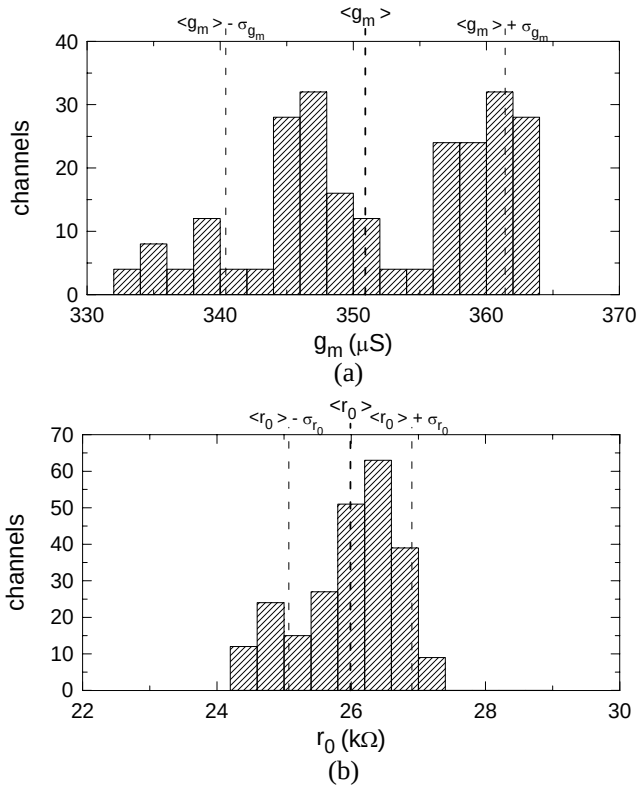

Figure 3. Homogeneity test of the small signal parameters ((a) Trasconductance, (b) Output resistance) of the on-chip front-end JFETS of the 3 cm^2 CDD

4. FEASIBILITY STUDY IN DIFFERENT APPLICATION FIELDS

In the previous section we have highlighted the main performance achieved with this kind of detector in terms of energy, position and time resolution. In the following

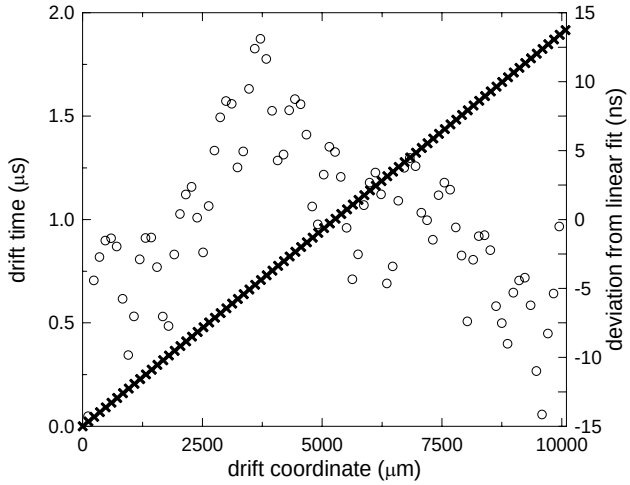

Figure 4. Measured drift time versus incident (drift) coordinate (crosses) and deviations from the linear fit (circles). The nominal drift field was 450 V/cm and the average drift velocity (from the linear fit) is 5.26 μm/ns.

we present some experiments performed to assess the suitability and potential of this kind of detectors in different imaging applications.

4.1. K-edge subtraction imaging

The abrupt change of the absorption coefficient of an element across its K-edge allows imaging the 2D distribution of selected elements in a sample by subtracting the transmitted image above and below the element's absorption edge [22]. The same technique can be used to enhance the contrast of selected elements in radiographic imaging and to obtain chemical information of the sample.

We have mapped the distribution of silver in a phantom composed of gold, indium, iron and silver. Fig. 5a shows the transmission image of the phantom illuminated by a 26.7 keV X-ray beam, above the K-edge of silver (25.51 keV) and below the K-edge of indium (27.94 keV). We acquired then transmission images at 24 keV (below the Ag K-edge) and 29.1 keV (above the In K-edge). Since the absorption coefficient of all the elements but silver is nearly constant changing from 24 keV to 26.7 keV, we can map the silver distribution in the phantom from the comparison of the two images at 24 and 26.7 keV. With the same method the indium distribution is obtained by comparing the images at 26.7 keV and at 29.1 keV. The superposition of the subtracted images gives the compositional map of the sample (for indium and silver in the present example).

A CDD-based system would allow a very fast 2D elemental mapping of centimeter-square area with spatial resolution of the order of 100 μm which is an alternative to elemental mapping techniques based on XRF and pencil beam scanning [23].

Profiting of the energy-resolving capability of the CDD the K-edge subtraction imaging technique can be performed also with conventional X-ray generators that provide a broadband spectrum, or with polychromatic sources, instead of stepping the primary beam energy with a monochromator.

4.2. Diffraction enhanced imaging

Conventional transmission imaging records the attenuation profile of a beam passing through the specimen under test therefore it is not able to distinguish among materials with similar density and, consequently, absorption coefficients. The diffraction pattern created by the interference of the coherently scattered photons at low angles (<10°) provides complementary information, related to the sample structure at atomic level, which is a unique signature characteristic of the material that has been irradiated. In the case of a structure with a short-range order, such as a biological tissue, the diffraction pattern is characterized by one or more smooth peaks at well-defined values of the momentum transfer $\chi = 1/\lambda \sin(\theta/2)$ where λ is the beam wavelength and θ is the scattering angle.

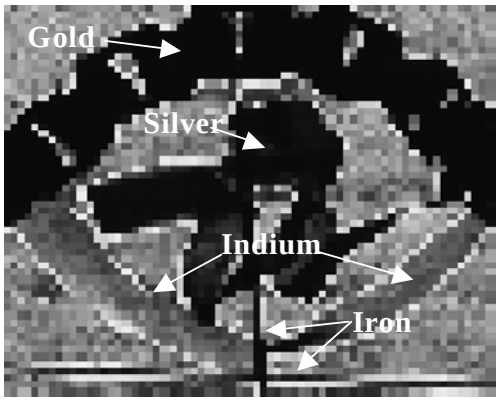

(a)

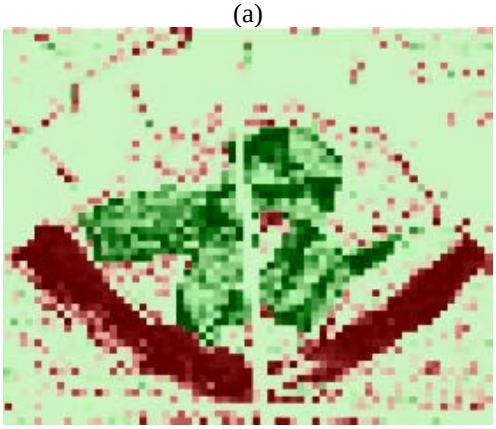

(b)

Figure 5. a) Radiography of a phantom composed by different elements (Silver, Gold, Iron and Indium). The energy of the incident beam was set equal to 26.7 keV (above the K-edge of Silver). b) Elemental map of indium (red) and silver (green) in the phantom obtained by means of K-edge subtraction imaging.

This is of particular interest in the case of mammography because healthy cells and cancer cells have a similar density, but show rather different diffractive effect on X-rays [24] (the maximum contrast between the scattered signal from normal breast tissue and carcinoma occurs at momentum transfer values of $\chi = 1.1\ nm^{-1}$ or $\chi = 1.7\ nm^{-1}$).

In order to probe the performance of the CDD in recording diffraction images we performed a measurement campaign at the SYRMEP beamline of Sincrotrone Trieste (Italy) [25] both with Perspex phantoms and meat samples.

Both diffraction and transmission images of the same sample have been acquired with the CDD. A goniometric cradle held the CDD at 9 degrees with respect to the incident beam direction for the acquisition of diffraction images. A multi-hole brass collimator (500 μm hole - 500 μm spacing) was placed in front of the CDD to acquire the diffraction images. The diffraction images were recorded by vertically scanning the sample in front of the beam. For each vertical position, two images, with a 500 μm horizontal displacement of the sample, were acquired, in order to cover the whole sample area. Two different beam energies have been used to define the required momentum

transfer values (18 keV for χ=1.1 nm^{-1} and 26 keV for χ=1.7 nm^{-1}).

For each detector pixel we selected the counts within an energy window of 5 keV centered at the photo-peak energy. All pixel counts corresponding to the same collimator hole were summed; hence, each line of a diffraction image consisted of 12 pixels 500 μm × 500 μm in size. Transmission images were recorded with the collimator removed and with the detector parallel to the primary beam. All the images were corrected for beam-intensity and detector-response non-uniformity by means of a flat-field image; for diffraction images the flat-field image was obtained with a uniform scatterer in front of the detector.

Fig. 6a shows one of the analyzed meat sample about 5 mm thick and selected for having two distinct regions of muscle (the bright area in the transmission image) and of fat (the dark area in the transmission image) which feature a scattered intensity distribution very close to tumor and normal tissue respectively. Fig. 6b shows the transmission image of this sample at 18 keV and Fig. 6c shows the diffraction image at the same energy. Figg. 6d and 6e shows the transmission and diffraction images, respectively, at 26 keV. The diffraction images were slightly misaligned with respect to the transmission ones. The contrast in the two diffraction images is reversed, as expected, because the diffraction signal of fat is higher than that of muscle at χ=1.1 nm^{-1}, while the opposite occurs at 1.7 nm^{-1} [26], thereby demonstrating the sensitivity to tissue type by appropriate choice of the momentum transfer to be imaged. The measured detail-to-background contrast in the transmission image at 18 keV (26 keV) is 0.29±0.02 (0.12±0.01). The contrast in the diffraction image increases to 0.48±0.03 and to 0.30±0.03 at 18 keV and 26 keV, respectively.

4.3. Compton electrons imaging

Several stacked layers of silicon CDDs constitute a very promising scatter detector for a Compton telescope for γ-ray imaging. Thanks to the high energy resolution of a CDD imager and to the relatively small Doppler broadening in silicon the original location of the γ-ray can in principle be reconstructed with sub-millimeter position resolution [27] for a wide range of gamma ray energies. This is of particular interest in the field of small-animal SPECT for in-vivo study of radiopharmaceuticals distribution. It should be pointed out that in a CDD the charge packets are drifted to one side of the detector chip that gives the additional advantages of a reduced number of output channels and of the possibility to stack several silicon layers with reduced amount of mass along the photon path. The fast trigger with a time resolution of few ns, needed for event coincidence, is provided by the signals induced on the back electrodes by the initial motion of the electron-hole track generated by the recoil electron.

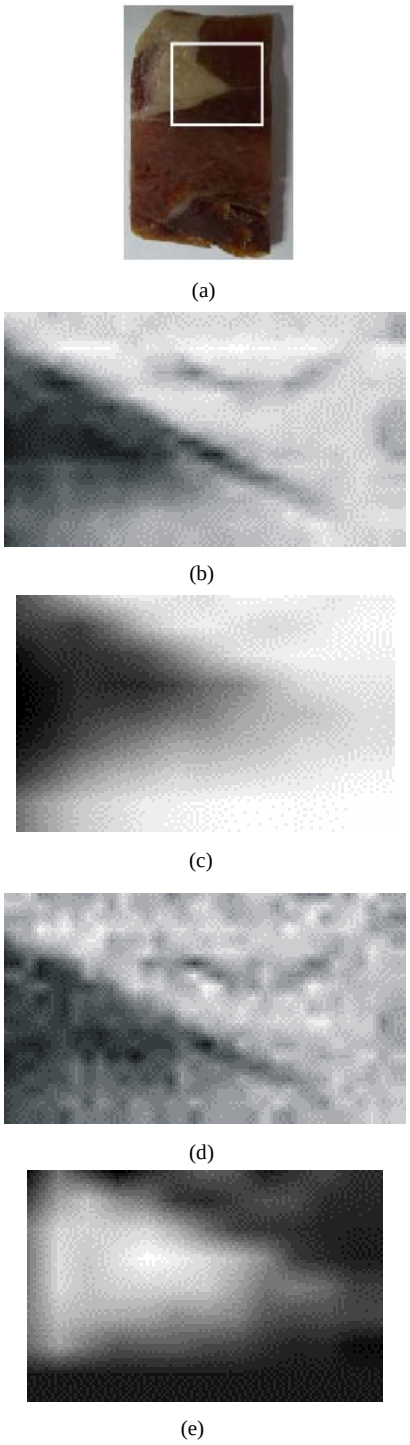

(a) (b) (c) (d) (e)

Fig. 6. a) Photograph of the analysed meat sample. The area delimited with the white line is the imaged one. b) Transmission image at 18keV. c) Diffraction image at 18keV. d) Transmission image at 26keV. e) Diffraction image at 26keV.

Electron tracking can significantly increase the sensitivity of Compton telescopes because the estimation of the recoil electron direction of the first Compton scatter can reduce the event cone to a short arc with uncertainty Δθ centered on the source direction. The possibility of

recording the electron track *within* the interaction layer would allow electron tracking not only for those electrons crossing more detection layers but also to low energy electrons, often totally absorbed in the interaction layer owing to the short electron range [28]. This is possible as the good energy and position resolution of the CDD allows imaging the 2D projection of the electron track and its ionization profile by sampling the charge deposited in each pixel. The projection of the initial direction of the recoil electron, the vertex of the interaction and the electron energy can therefore be more precisely estimated for wide range of Compton electron energies leading to improved resolution and efficiency. This would be an essential upgrade in the case of low gamma energies (<0.5 MeV).

We carried out preliminary measurements with a ^{22}Na source. The induction signal picked up at the back contact provided the interaction time (and the start of the electron drift) with a measured time jitter of about 6 ns FWHM (back contact of about 1.6 mm × 1.7 mm). Figs. 7a, 7b, 7c show selected examples of recorded tracks. In each figure the left inset shows the pixilated (120μm×120μm pixel size) image of the Compton electron ionization track. Pixel colors correspond to the deposited energy (in keV) according to the shown color map. The right inset shows the estimated specific energy loss after least square fit to the theoretical curve (solid line) that gives the estimate of the initial Compton electron energy. Fig. 7a shows the case in which a 415 keV electron is fully absorbed in the silicon detector. The marked increase of the deposited energy near the end of the track is clearly visible. Fig. 7b shows the case in which the ionization track appears inside the detector volume and stops at the edge of the active area or beyond it with partial charge loss. Fig. 7c shows a different case in which an energetic electron (915 keV) crosses the detector thickness and escapes through the surface with a residual energy of about 760 keV.

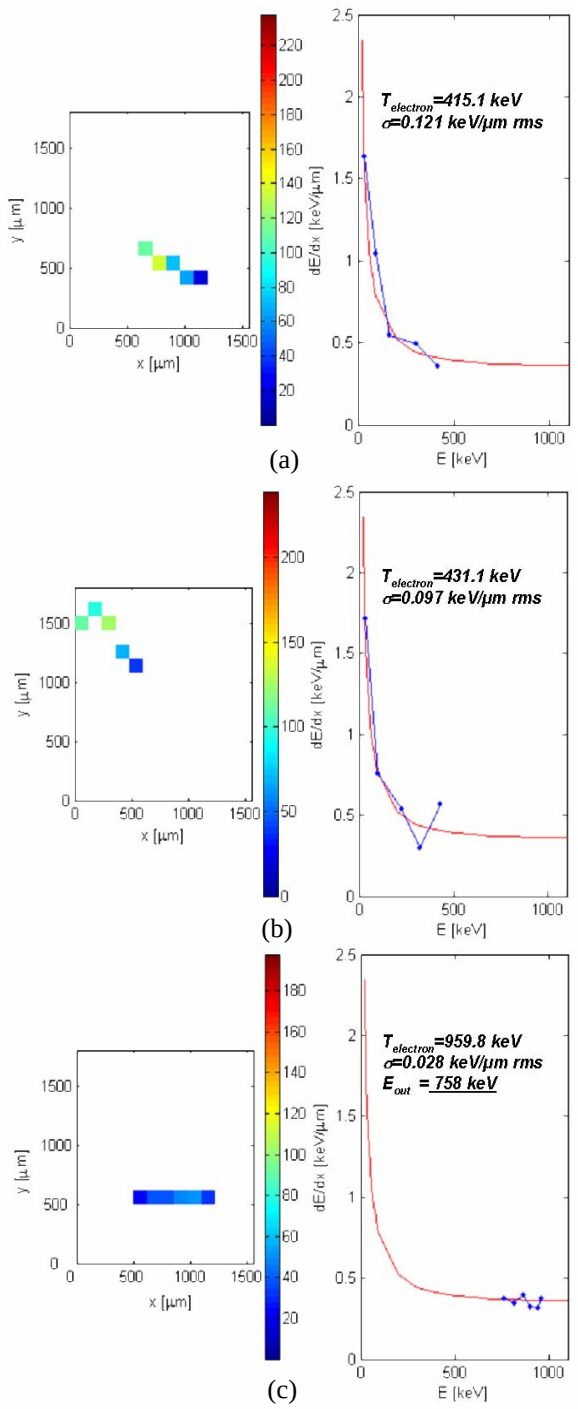

Figure 7. Selected examples of recorded Compton electron tracks originated by γ-rays coming from a ^{22}Na source. The color map is referred to the left inset and shows the deposited energy (keV units). a) A 415 keV electron is fully absorbed in the silicon detector. b) The ionization track appears inside the detector volume and stops at the edge of the active area or beyond it with partial charge loss. c) An energetic electron (915 keV) crosses the detector thickness and escapes through the surface with a residual energy of about 760 keV.

Acknowledgments

A.C. wish to thank SNIC Symposium organizers for the invitation. The authors also acknowledge the staff of the Max Planck Institut Halbleiterlabor in Munich together with H. Soltau, P. Holl, and the staff of PNSensor GmbH in Munich for detector production. We also thank D. Arcieri for the help in the development of the DAQ system and D. Fugazza, C. Mantovani and A. Vescovi for the help in the experimental measurements. We are in debt to the staff of the SYRMEP beamline at Elettra Sincrotrone Trieste for the kind hospitality.

Work fully supported by INFN, Sezione di Milano, Italy.

References

[1] E.Gatti, P.Rehak, "Semiconductor Drift Chamber: an application of a novel charge transport scheme", *Nucl. Instr. and Meth.* A225, pp. 608-614, 1984.

[2] A. Rashevsky et al., “Characteristics of the ALICE Silicon Drift Detector”, Nucl. Instr.and Meth. A 461, pp. 133-138, 2001.
[3] R.Bellwied et al., STAR SVT Group, “Development of large linear silicon drift detectors for the STAR experiment at RHIC”, Nucl. Inst. and Meth., A377, pp. 387-392, 1996.
[4] E. Gatti, P. Rehak, “Review of semiconductor drift detectors”, Nucl. Instr. and Meth. A541 pp. 47-60, 2005.
[5] P. Lechner, S. Eckbauer, R. Hartmann, S. Krisch, D. Hauff, R. Richter, H. Soltau, L. Strüder, C. Fiorini, E. Gatti, A. Longoni, M. Sampietro, “Silicon drift detectors for high resolution room temperature X-ray spectroscopy,” Nucl. Instr. Meth., vol. A 377, pp. 346-351, 1996.
[6] P.Lechner, C.Fiorini, R.Hartmann, J.Kemmer, N.Krause, P.Leutenegger, A.Longoni, H.Soltau, D.Stötter, R.Stötter, L.Strüder, U.Weber, "Silicon drift detectors for high count rate X-ray spectroscopy at room temperature", Nucl. Instr. Meth., vol. A 458, pp. 281-287, 2001.
[7] P. Lechner, W. Buttler, C. Fiorini, R. Hartmann, J. Kemmer, N. Krause, P. Leutenegger, A. Longoni, H. Soltau, D. Stötter, R. Stötter, L. Strüder, U. Weber, ”Multichannel silicon drift detectors for x-ray spectroscopy”, Proc. SPIE 4012, pp. 592-599, 2000.
[8] P. Lechner, A. Pahlke, H. Soltau, ”Novel high-resolution silicon drift detectors”X-Ray Spectrom. 33, pp. 256-261, 2004.
[9] A.Castoldi, P.Rehak, P.Holl, ”Signal charge sharing in multilinear drift detectors: Design and experimental characterization”, IEEE Trans. Nucl. Science 44, pp. 134-141, 1997.
[10] A. Castoldi, C. Guazzoni, A. Longoni, E. Gatti, P. Rehak, L. Strüder, "Conception and design criteria of a novel silicon device for the measurement of position and energy of X-rays", IEEE Trans. Nucl. Sci., vol. 44, pp. 1724-1732, 1997.
[11] Patents: US 6,249,033, EP0862226.
[12] L. Strüder, H. Bräuninger, U. Briel, R. Hartmann, G. Hartner, D. Hauff, N. Krause, B. Maier, N. Meidinger, E. Pfeffermann, M. Popp, C. Reppin, R. Richter, D. Stötter, J. Trümper, U. Weber, P. Holl, J. Kemmer, H. Soltau, A. Viehl, C. v. Zanthier, "A 36 cm^2 large monolytic pn-charge coupled device X-ray detector for the European XMM satellite mission", Rev Sci Instrum., vol. 68, pp. 4271-4274, 1997.
[13] A. Castoldi, A. Galimberti, E. Gatti, C. Guazzoni, P.Rehak, and L.Strüder, "X-ray 2-D Position-Sensing with Multi-Linear Silicon Drift Detectors", IEEE Trans. Nucl. Sci., Vol. 53 (2), pp. 601-606, 2006.
[14] A. Castoldi, E. Gatti, C. Guazzoni, “Fast Triggering in Silicon Drift Detectors by means of Holes’ Induction”, Nucl. Instr. and Meth. A518, pp. 429-432, 2004.
[15] E. Gatti, P. Rehak, M. Sampietro, "Double particle resolution in Silicon Drift Detectors", Nucl. Instr. and Meth. A274, pp. 469-476, 1989.
[16] A.Castoldi, C.Guazzoni, "A New Position Sensing X-Ray Detector: Working Principle And Experimental Results", IEEE Trans. Electron Device, Vol.46, no.2, p.329-334, Feb. 1999.
[17] A. Castoldi, C. Guazzoni, P. Rehak, L. Strüder, "Spectroscopic-grade X-ray imaging up to 100 kHz frame rate with Controlled-Drift Detectors" IEEE Trans. Nucl. Sci., Vol. 48, No. 4, pp. 982-986 , August 2001.
[18] A. Castoldi, G. Cattaneo, A. Galimberti, C. Guazzoni, P. Rehak, L. Strüder, "Room-temperature 2-D X-ray imaging with the Controlled-Drift Detector", IEEE Trans. Nucl. Sci., Vol. 49, No. 3, pp. 989-994, June 2002.
[19] A. Castoldi, A. Galimberti, C. Guazzoni, P. Rehak, L. Strüder, R. H. Menk, “Energy-resolved X-ray radiography with controlled-drift detectors at Sincrotrone Trieste”, Nucl. Instr. Meth., Vol .A510, pp. 57-62, 2003.
[20] A. Castoldi, A. Galimberti, “Multichannel Acquisition System for High-Resolution Position-Sensing Silicon Drift Detectors”, IEEE Trans. Nucl. Sci., Vol. 53, pp. 526-531, 2006.
[21] A. Castoldi, A. Galimberti, C. Guazzoni, L.Strüder, *"Time-Resolved X-ray Spectroscopic Imaging with Novel Silicon Drift Detectors"*, IEEE Trans. Nucl. Sci., Vol. 53(1), Feb. 2006, pp. 373-377.
[22] R. E. Alvarez and A. Macovski, "Energy selective reconstructions in x-ray computerized tomography", Phys. Med. Biol. Vol. 21, pp. 733-44, 1976.
[23] A.Longoni, C. Fiorini, C. Guazzoni, S. Buzzetti, M. Bellini, L. Strüder, P. Lechner, A. Bjeoumikov, J. Kemmer, "A novel high resolution XRF spectrometer for elemental mapping based on a monolithic array of Silicon Drift Detectors and on a polycapillary X-ray lens", X-ray Spectrometry, Vol. 34 (5), pp. 439-445, 2005.
[24] G Kidane et al. "X-ray scatter signatures for normal and neoplastic breast tissues", *Phys Med Biol* 1999: 44; 1791-1802.
[25] Elettra Sincrotrone Trieste, Strada Statale S.S. 14, km 163.5, 34012 Basovizza, Trieste, Italy, http:\\www.elettra.trieste.it
[26] J. A Griffiths, R. D. Speller, G. J. Royle, J. A. Horrocks, A. Olivo, S. Pani, R. Longo, D. Dreossi, D. P. Clifford and A. M. Hanby, “X-Ray Diffraction CT of Excised Breast Tissue Sections: First Results from Elettra”, 2003 IEEE Nuclear Science Symposium and Medical Imaging Conference Conference Records, Portland Oregon, USA, 2003.
[27] T. Conka-Nurdan, K. Nurdan, F. Constantinescu, B. Freisleben, N.A. Pavel, A.H. Walenta, "Impact of the Detector Parameters on a Compton Camera", IEEE Trans.Nucl.Sci., Vol. 49, no. 3, pp. 817-821, 2002.
[28] O'Neill TJ, Ait-Ouamer F, Schwartz I, Tumer OT, White RS, Zych AD, Compton recoil electron tracking with silicon strip detectors, IEEE Trans. Nucl. Sci. 1992: 39; 629-634.